Research Paper

Novel skin patch combining human fibroblast-derived matrix and ciprofloxacin for infected wound healing

Muhammad Suhaeri[1,2,3,†], Mi Hee Noh[4,†], Ji-Hoi Moon[5], In Gul Kim[1], Seung Ja Oh[1], Sang Su Ha[1,6], Jong Ho Lee[1], Kwideok Park[1,6, ✉]

1. Center for Biomaterials, Korea Institute of Science and Technology, Seoul 02792, Republic of Korea
2. Unit of Education, Research, and Training, Universitas Indonesia Hospital, Universitas Indonesia, Depok 16424, Indonesia
3. Medical Technology Research Cluster, Indonesia Medical Education and Research Institute, Faculty of Medicine, Universitas Indonesia, Jakarta Pusat 10430, Indonesia
4. Department of Biomedical Science, Graduate School, Kyung Hee University, Seoul 02447, Republic of Korea
5. Department of Maxillofacial Biomedical Engineering, School of Dentistry/Department of Life and Nanopharmaceutical Sciences, Kyung Hee University, Seoul 02447, Republic of Korea
6. Division of Bio-Medical Science and Technology, KIST School, Korea University of Science and Technology (UST), Seoul 02792, Republic of Korea

†These authors contributed equally

✉ Corresponding author: Kwideok Park, Ph.D. E-mail: kpark@kist.re.kr; Tel: +82-2-958-5288; Fax: +82-2-958-5308

Abstract

Skin injuries are frequently encountered in daily life, but deep wounds often poorly self-heal and do not recover completely. In this study, we propose a novel skin patch that combines antibiotic, cell-derived extracellular matrix (ECM) and biocompatible polyvinyl alcohol (PVA) hydrogel.

Methods: Decellularized human lung fibroblast-derived matrix (hFDM) was prepared on tissue culture plate (TCP) and PVA solution was then poured onto it. After a freeze-thaw process, PVA was peeled off from TCP along with hFDM tightly anchored to PVA. Subsequently, ciprofloxacin (Cipro)-incorporated PVA/hFDM (PVA/Cipro/hFDM) was fabricated via diffusion-based drug loading.

Results: In vitro analyses of PVA/Cipro/hFDM show little cytotoxicity of ciprofloxacin, stability of hFDM, rich fibronectin in hFDM, and good cell attachment, respectively. In addition, hFDM proved to be beneficial in promoting cell migration of dermal fibroblasts and human umbilical vein endothelial cells (HUVECs) using transwell inserts. The antibacterial drug Cipro was very effective in suppressing colony growth of gram-negative and -positive bacteria as identified via an inhibition zone assay. For animal study, infected wound models in BALB/c mice were prepared and four test groups (control, PVA, PVA/Cipro, PVA/Cipro/hFDM) were administered separately and their effect on wound healing was examined for up to 21 days. The results support that Cipro successfully reduced bacterial infection and thus encouraged faster wound closure. Further analysis using histology and immunofluorescence revealed that the most advanced skin regeneration was achieved with PVA/Cipro/hFDM, as assessed via re-epithelialization, collagen texture and distribution in the epidermis, and skin adnexa (i.e., glands and hair follicles) regeneration in the dermis.

Conclusion: This work demonstrates that our skin patch successfully consolidates the regenerative potential of ECM and the antibacterial activity of Cipro for advanced wound healing.

Key words: wound healing, skin patch, human fibroblast-derived matrix, ciprofloxacin, polyvinyl alcohol hydrogel

Introduction

Skin is the largest organ in the human body and has special functions such as physically blocking pathogens, excreting metabolic wastes, maintaining body moisture, and regulating body temperature [1].

Once injured, a cascade of wound healing processes immediately takes place. Wound healing is a complicated but highly regulated biological event involving specific immune cells (leukocytes,

macrophages), tissue cells (fibroblasts, keratinocytes, endothelial cells), and a variety of cytokines or growth factors (TNF-α, TGF-β, PDGF, VEGF, FGF). Eventually, wounds recover structural integrity and normal functions as a result of spatio-temporally controlled interactions among cells, growth factors, and extracellular matrix (ECM).

Among numerous cases of skin injuries, bacterial infection is often problematic and can lead to a chronic wound. This happens because the toxins produced by bacteria trigger inflammation by stimulating inflammatory cells to release pro-inflammatory cytokines [2]. For this reason, wound dressings with antibacterial activity that can suppress infections and consequently facilitate wound healing are extensively investigated. One study developed a hydrogel-based wound dressing with different ratios of Ag/graphene. In a rat wound model, the composite hydrogels were able to accelerate the healing process and as a result reconstructed a thick epidermis layer [3]. Another hybrid dressing of antibiotic-loaded poly(DL-lactic-co-glycolic acid) and spongy collagen also supported early onset of wound healing by slowly releasing gentamicin from the dressing [4]. These examples illustrate the benefits of wound dressings equipped with antibacterial agents for a better healing outcome.

Similarly, ECM is considered a key player in skin wound healing progression involving ECM degradation, new ECM synthesis, and ECM remodeling. Cell-ECM interactions are predominantly mediated via cell surface receptor integrins that bind to ECM. Recent studies have reported that interactions between cells and wound-associated ECMs, such as fibrin, fibronectin, and collagen, have a great influence on wound healing [5]. They serve as provisional matrix proteins in wound repair. In addition, ECM interacts with growth factors. These growth factors could recognize ECM and bind to ECM in order to prevent them from early degradation [6]. Cell attachment to ECM could enhance the growth factors production mechanisms of cells.

Considering the significant role of ECM, Cho et al. combined human adipose-derived soluble ECM with methylcellulose to make an injectable thermosensitive hydrogel [7]. By embedding stem cells in this hydrogel and applying them to *in vivo* cutaneous wounds, they noticed rapid healing marked by re-epithelialization and new blood vessel formation. Similarly decellularized ECM derived from human placenta was fabricated as a scaffold for treatment of a full thickness wound model [8]. The outcome shows that the ECM scaffold provided the cells with a supportive microenvironment and thus promoted better wound healing.

In this study, we have attempted to produce a novel skin wound patch that physically combines cell-derived ECM and an antibacterial agent together. The hypothesis is that our patch retains both functions and thus provides more advanced therapeutic benefits toward skin wound healing. For this purpose, ciprofloxacin was selected as an antibiotic due to its extensive use in wound healing applications and wide spectrum activity against gram-positive and -negative bacteria [9]. Human lung fibroblast-derived matrix (hFDM) was chosen to recapitulate the native ECM microenvironment upon the mounting benefits of cell-derived matrices in the field of tissue engineering and regenerative medicine [10]. To deliver ciprofloxacin and hFDM, a hydrogel dressing based on polyvinyl alcohol (PVA) was employed due to its humid environment, excellent biocompatibility, and viscoelastic property [11]. More importantly, without the use of chemicals, PVA can be crosslinked physically via freeze-thawing processes. Herein, we developed a ciprofloxacin-loaded PVA/hFDM patch and investigated its efficacy for wound healing using infected skin wound animal models. This work demonstrates that PVA/Cipro/hFDM is effective as a skin patch in facilitating wound healing, especially skin adnexa (i.e., glands, hair follicles) regeneration and, therefore, it can be a promising candidate for advanced skin regeneration.

Materials and Methods

Fabrication of PVA/hFDM membrane

To prepare a human lung fibroblast-derived matrix (hFDM), human lung fibroblasts (WI-38, CCL-75; ATCC) were seeded (2×10^4/cm^2) in 24-well plate and cultured for 7 days in Dulbecco's modified Eagle's medium (DMEM) supplemented with 10% fetal bovine serum (FBS), 100 U/mL penicillin, and 100 µg/mL streptomycin under normal culture condition (5% CO_2, 37 °C). The medium was changed every 2-3 days. After several washings with phosphate buffered saline (PBS), cells were subject to decellularization using 0.25% Triton-X 100 and 50 mM NH_4OH (221228, Sigma), followed by incubation with 50 U/mL DNase I (18047-019, Invitrogen) and 2.5 µL/mL RNase A (12091-039, Invitrogen) at 37 °C for 2 h. Once the decellularized hFDM was rinsed with PBS several times, 7% (w/v) aqueous polyvinyl alcohol (PVA) (MW 146,000-186,000; 363065, Sigma) was added onto the hFDM. Crosslinking of PVA hydrogel was carried out via storage at -20 °C for 24 h and subsequent thawing at room temperature for 1 h. PVA hydrogel coupled with hFDM was then carefully peeled off from the tissue culture plate using forceps and transferred to a new plate. To evaluate the stable anchorage of hFDM to PVA, this PVA/hFDM

membrane was ultrasonicated in an ultrasonic cleaner (Powersonic 603; Kleentek) with the highest power setting for 5 min at 25 °C. Such operation was repeated for up to 3 cycles. For each cycle, the condition of hFDM was evaluated under a light microscope (Axio Vert.A1; Carl Zeiss).

Ciprofloxacin loading and release test

To incorporate an antibiotic drug, ciprofloxacin, into the PVA/hFDM membrane, different ciprofloxacin (17850, Sigma) concentrations (1, 10, and 20 mg/mL) were prepared in 0.1 N hydrochloric acid (HCl). To each of these solutions (2 mL each), PVA/hFDM membrane was soaked and incubated for 30 min at 37 °C. Then, ciprofloxacin-loaded PVA/hFDM (PVA/Cipro/hFDM) was carefully removed and the remaining solutions were weighed to measure changes in weight. The percentage of ciprofloxacin incorporated was calculated by the weight difference of solutions before and after ciprofloxacin loading. For the release study of ciprofloxacin, PVA/Cipro/hFDM was incubated in PBS at 37 °C and aliquots were taken at specific time points, along with subsequent replacement of fresh PBS. Measurement of ciprofloxacin content was carried out using a spectrophotometer at 355 nm.

Examination of cell viability and adhesion

Cell viability of the PVA-based membranes was evaluated using a LIVE/DEAD Viability/ Cytotoxicity Kit (MP03224; Invitrogen) according to the manufacturer's instruction. PVA and PVA/Cipro were initially coated with 0.5% (w/v) gelatin for 30 min to allow cell attachment, because of poor cell attachment to PVA itself. We compared gelatin-coated PVA (equally treated with 0.1 N HCl solution) and 1 mg/mL ciprofloxacin-treated PVA (PVA/Cipro) against TCP (control). Mouse fibroblasts (NIH3T3, CRL-1658; ATCC) were then seeded (2×10^4/cm^2) and cultured for 24 h. Once the medium was aspirated, the cells were incubated with LIVE/DEAD solution for 30 min at 37 °C, and mounted on a glass coverslip. Live and dead cells were identified by green and red fluorescence, respectively, using a confocal laser scanning microscope (Fluo View FV1000; Olympus). The percentage of cell viability was calculated from five random images (1×10^5 µm^2) by comparing the number of green and red cells via image J (NIH) from three replicates of each group. In addition, to assess the quality of PVA/hFDM during the drug loading process, PVA/hFDM was treated with 0.1 N HCl and examined for ECM quality and cell adhesion, along with PBS-treated PVA/hFDM as a control group.

Immunofluorescence

Samples were initially fixed using 4% formaldehyde for 30 min at room temperature,

permeabilized with 0.1% Triton-X 100, and blocked by 1% bovine serum albumin (BSA) for 1 h at room temperature. At each step, samples were washed three times with PBS. They were then incubated with primary antibodies for 1 h at 4 °C, rinsed several times with PBS, and subsequently treated with secondary antibodies for 1 h at room temperature. After a thorough washing, the samples were mounted on microscope cover glasses using vectashield® mounting medium with 4', 6-diamidino-2-phenylindole (DAPI) (H1200; Vector Lab.) for nucleic labeling and fluorescence images were then collected using a confocal laser scanning microscope (Carl Zeiss). The primary antibodies were mouse anti-fibronectin (SC-8422; Santa Cruz Biotechnology), mouse monoclonal anti-vinculin (sc-73614; Santa Cruz), and rabbit polyclonal anti-connexin 43 (ab11370; abcam). The secondary antibodies were Alexa Fluor 488-conjugated goat anti-mouse IgG (A11001; Invitrogen) and rhodamine red-X goat anti-rabbit (R6394, Invitrogen), while cell cytoskeleton f-actin was stained using rhodamine phalloidin (R415; Life Technology). The cell area was analyzed by manually selecting the cell borders via image J. Similarly, cell density was also calculated from the images of nuclei staining. A total of 50 cells was chosen from three replicates of each group.

Chemotaxis effect of hFDM

To prepare proper samples for chemotaxis study, hFDM was freeze-dried and digested using 1 mg/mL pepsin in 0.01 N HCl at 37 °C for 48 h. This hFDM suspension was then neutralized via 0.1 N NaOH and the protein content was quantified using a BCA protein assay kit (23250; Thermo Scientific). For chemotaxis effect, three different concentrations (25, 50, and 100 µg/mL) of soluble hFDM were prepared in DMEM without the addition of FBS. For comparison, DMEM with 10% FBS served as a positive control and without serum (0% FBS) was a negative control. Cell migration across transwell inserts was investigated using two types of cells, human umbilical vein endothelial cells (HUVECs) (C2517A; Lonza) and human dermal fibroblasts (HDFs) (CRL-2522; ATCC). Cells were seeded at 5×10^4 cells in 8 µm pore diameter transwells (353182; Falcon) filled with medium without FBS. The lower chamber was occupied with hFDM suspension, negative control, or positive control. The overall experimental schematic is shown in **Figure S1**. Cell migration was allowed for 3 and 6 h with HDFs and HUVECs, respectively. Then, cells in the lower chamber were stained with 0.2% (w/v) crystal violet and counted under a light microscope (Axio Vert.A1; Carl Zeiss). In each well, five random images (3×10^5 µm^2) from three replicates of each group were taken

and the number of cells was determined.

Gap junctional communication of HUVECs

HUVECs and red fluorescence protein-expressing HUVECs (RFP-HUVECs, cAP-0001RFP; Angio-Proteomie) were separately seeded (2×10⁴ cells/cm²) on gelatin-coated coverslips and hFDM, respectively. Once they reached confluence, HUVECs were labeled with 4 µM calcein AM (C1430; Invitrogen) for 30 min and washed three times with PBS. The labeled HUVECs were then trypsinized and transferred for co-culture with RFP-HUVECs. Calcein AM-labeled HUVECs on gelatin were transferred to RFP-HUVECs seeded on gelatin, and those on hFDM were also moved to RFP-HUVECs on hFDM. Co-cultured cells were incubated for 24 h and observed under a fluorescence microscope for calcein dye transfer. Calcein dye-transferred cells were determined by counting the number of RFP-HUVECs (red) with calcein dye (green), and the result was marked as the percentage of RFP-HUVECs stained with green dye collected from at least 50 RFP-HUVECs in each replicate (n = 3). In addition, five random immunofluorescence images (1×10⁵ µm²) of connexin 43 (Cx43)-positive cells were analyzed via image J by thresholding the Cx43 signals to obtain their area. The average Cx43 positive area was normalized to the cell area. Each group contained three replicates.

Antibacterial activity *in vitro*

A total of four gram-negative and -positive bacterial strains were employed for zone inhibition assay: *Escherichia coli* (25922; ATCC), *Pseudomonas aeruginosa* (27853; ATCC), *Staphylococcus epidermidis* (12228; ATCC), and *Staphylococcus aureus* (25923; ATCC). They were grown aerobically in Mueller-Hinton broth (Difco Laboratories, Detroit, MI) at 35 °C for 18 h. A disc diffusion test was carried out according to the guidelines of the Clinical and Laboratory Standards Institute using Mueller-Hinton Agar [12]. Briefly, the agar surface was inoculated by using a swab dipped in the bacterial cell suspension with a turbidity of 0.5 McFarland standard units and then allowed to dry for approximately 5 min. The test samples (PVA, PVA/Cipro, PVA/Cipro/hFDM) were placed on the agar surface and the susceptibility plates were incubated at 35 °C for 16-18 h. Especially for PVA/Cipro/hFDM, the sample was positioned on the agar plate so that the hFDM side directly contacted bacteria culture. Inhibition zones around the discs were measured in millimeter using a ruler.

Infected skin wound model *in vivo*

Female 6-8-week-old BALB/c mice were used for animal experiments following the guidelines of the Institutional Animal Care and Use Committee, Kyung Hee University. The wound infection model described herein is in accordance to the literature by Kopecki et al [13]. A single full-thickness wound was made in the dorsal region of the mice, followed by bacterial infection of *S. aureus* (10⁷ CFU/100 µL) administered via gauze to the wound area. 6 h post-bacterial infection, the gauze was removed and the wounds were treated with PVA, PVA/Cipro, or PVA/Cipro/hFDM. The surgical procedure for patch application to the wounded mouse model is shown in **Figure S2**. The patches were replaced every 3-4 days. Infected wound without any treatment was used as a control. Bacterial swabs from the injury site were collected 6 h post-treatment and bacterial viability was examined by colony forming unit assay. Progression of wound healing was monitored by photographic records at specific time points and presented quantitatively as the percentage of wound size relative to the original wound scale. In each group, the animals were sacrificed on day 21 (n = 3).

Histology

Skin tissue samples from wound areas were harvested and fixed in 10% formalin. After imbedding in paraffin block, they were bisected across the wound site or cross-sectioned along the tissue. Hematoxylin and eosin (H&E) staining was carried out to evaluate morphological characteristics of the epidermis and dermis regions. The thickness of the epidermis was measured at 15 and 21 days using microscopic images of H&E staining, based on three replicates per animal and each replicate with three random epidermal regions. Similarly, microvessel density was also determined from tissue samples on day 21 by counting the number of microvessels from three different regions in the regenerated dermis layer and by averaging them per unit area. Collagen deposition and its distribution were observed via Masson's trichrome staining. In addition, identification of Cx43 protein was carried out using immunohistochemistry of histological samples with a heat-mediated antigen retrieval process. Briefly, the samples were deparaffinized and rehydrated by sequential immersion in xylene, ethanol, and water. Antigen retrieval was carried out by heating the hydrated samples at 98 °C for 2 min via microwave. Then, the samples were subject to immunofluorescence of Cx43 and quantitatively analyzed as described earlier. The quantity of Cx43 was calculated from five random images with three replicates of each group (n = 3). In addition, for neovascularization analysis, immuno-fluorescence of CD31 (an endothelial cells marker) was carried out: the primary antibody was rabbit polyclonal anti-CD31 (ab28364) diluted in 1% BSA at 1:200; the secondary antibody used was Alexa Fluor® 594-conjugated donkey anti-rabbit IgG (H+L)

(A21207) diluted in 1% BSA at 1:200.

Statistics

All data presented are mean ± standard deviation. Statistical analysis was performed using a two-tailed (α = 0.05) Student's t-test for the experiments with two experimental groups. One-way ANOVA with a post hoc Tukey's multiple comparison test was applied for more than three test groups. A statistically significant difference is denoted as * ($p < 0.05$), ** ($p < 0.01$), or *** ($p < 0.001$).

Results

Fabrication and characterization of PVA/Cipro/hFDM

Figure 1A depicts a schematic of the overall procedure for combining PVA hydrogel with hFDM. We prepared hFDM as previously reported [14], and confirmed the presence of the fibrillar structure of ECM via optical microscopy (**Figure 1B**). As a next step, PVA solution was poured onto hFDM and then subjected to freeze-thaw for the induction of physical crosslinking of the hydrogel [15]. A thin membrane of PVA/hFDM was peeled off using forceps without leaving hFDM on the plastic substrate (**Figure 1B**, inset). This process securely couples hFDM with PVA hydrogel. When hFDM was stained against fibronectin, it was clearly visible that hFDM was successfully transferred from TCP to PVA hydrogel (**Figure 1C**). Additionally, a cross-sectional image demonstrates a nicely formed interface between hFDM and PVA located on the surface of the hydrogel (**Figure 1D**). When we evaluated the stability of hFDM in the PVA/hFDM membrane via ultrasonication: even after 3 cycles of high-power ultrasonication, the anchorage of hFDM to PVA was still intact (**Figure S3**). Upon successful coupling of PVA and hFDM, we incorporated ciprofloxacin into PVA/hFDM in order to fabricate PVA/Cipro/hFDM. It seems that inclusion of ciprofloxacin inside PVA hydrogel is based on drug uptake during the hydrogel swelling process. Our results demonstrate that the drug loading efficiency was around 8%, independent of the initial ciprofloxacin concentration (**Figure 1E**). In addition, we found that the higher initial loading concentration, the faster ciprofloxacin release (**Figure 1F**).
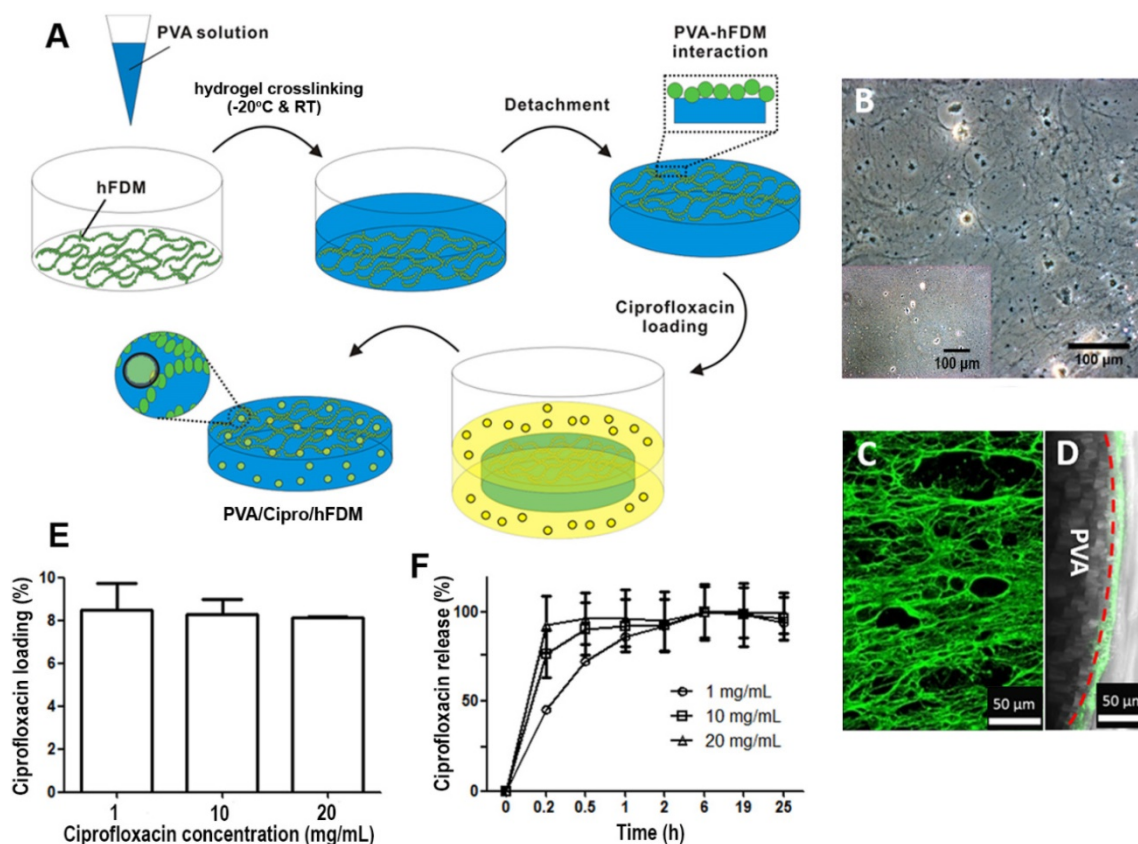

Figure 1. Preparation of PVA/hFDM and ciprofloxacin-loaded PVA/hFDM. (A) Schematic illustration of the overall process in fabricating PVA/hFDM and ciprofloxacin-loaded PVA/hFDM. **(B)** Microscopic image of decellularized hFDM on TCP and the surface of TCP right after the transfer of hFDM into PVA hydrogel. Scale bar is 100 µm. **(C)** Immunofluorescence of FN in the PVA/hFDM. **(D)** Cross-sectional view of the interface (dashed red line) between PVA and hFDM. Scale bar is 50 µm. **(E)** Loading of ciprofloxacin with different initial concentrations into PVA hydrogel and **(G)** the release profile over 24 h in PBS at 37 °C. FN: fibronectin; hFDM: human lung fibroblast-derived matrix; PVA: polyvinyl alcohol; TCP: tissue culture plastic.

Effects of ciprofloxacin on cells and hFDM

Cell viability and cell adhesion were examined because the use of acidic condition (0.1 N HCl) in preparing ciprofloxacin-loaded PVA membrane may be harmful to cells. At 24 h post-seeding, the two treatment groups (PVA and PVA/Cipro) exhibited few dead cells (**Figure 2A**), similar to that of control (**Figure 2A**, inset). The percentage of cell viability was comparable across groups (**Figure 2B**), indicating that the current platform is barely cytotoxic even in the presence of acidic ciprofloxacin solution. Another issue is the effect of the acidic condition on the biofunctionality of hFDM. We prepared PBS-treated and 0.1 N HCl-treated PVA/hFDMs, respectively and examined fibronectin, a major ECM component. Our result suggests that acidic solution treatment does not compromise the ECM protein contained in the hFDM (**Figure 2C**).

Further analysis of hFDM as a substrate of cell adhesion showed that, as shown in **Figure 2D**, cells attached well and spread on both groups as evidenced by focal adhesion molecule (vinculin, green) and f-actin (red), respectively. Analysis of cell spreading area and cell density unveiled no significant difference between PBS-treated and 0.1 N HCl-treated PVA/hFDM (**Figure 2E-F**). These findings demonstrate that the biofunctionality of hFDM, such as cell adhesion [16], is maintained after exposure to acidic condition during the ciprofloxacin loading process.

Chemotaxis effect of hFDM

To evaluate whether hFDM has a chemotactic activity, hFDM suspension was harnessed to investigate the motility of HUVECs and HDFs, respectively. Our results revealed that hFDM suspension could enhance cell motility as assessed via transwell migration assay (**Figure 3A-B**).
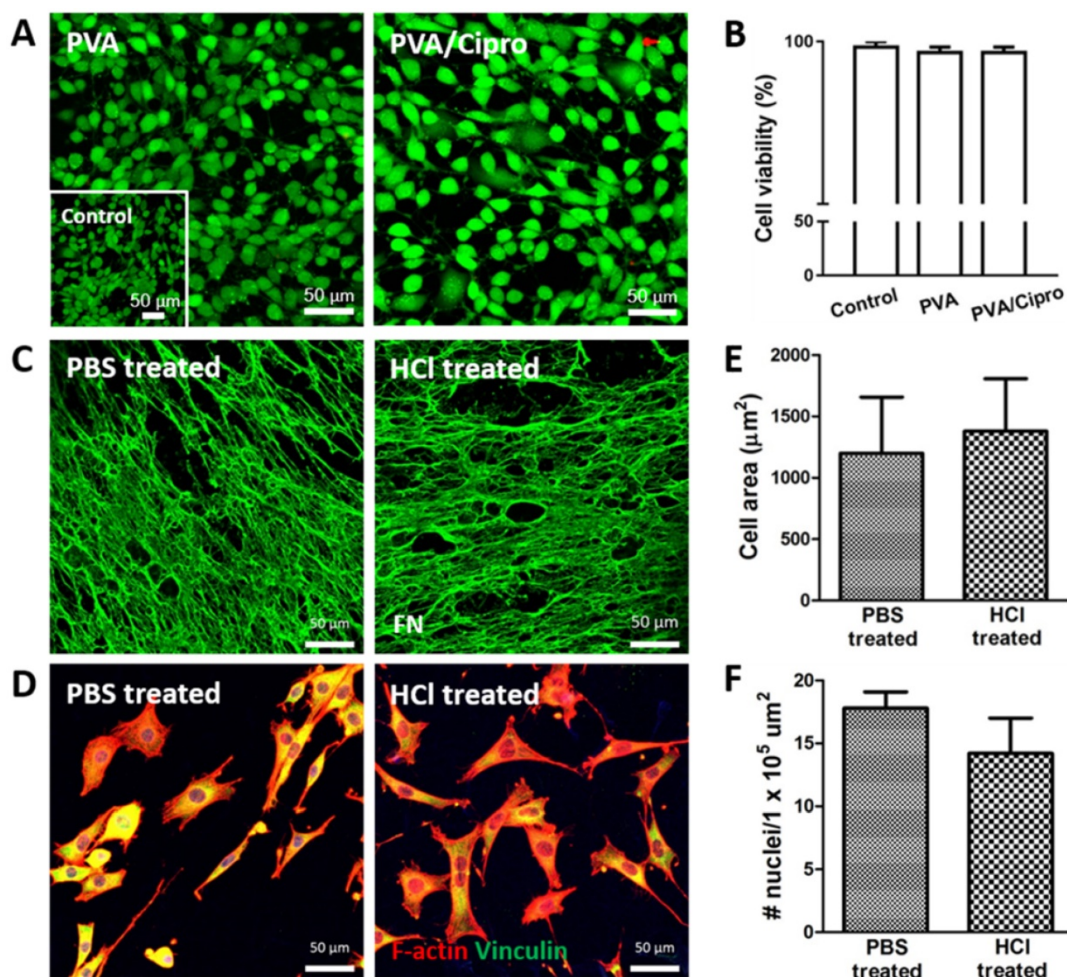

Figure 2. Characterization of PVA-based membranes. (A) Cell viability test of mouse fibroblasts after 24 h culture on gelatin coated-PVA (treated with 0.1 N HCl) and gelatin-coated PVA/Cipro (treated with 1 mg/mL ciprofloxacin) as evaluated via live/dead assay. Inset shows the cells cultured on TCP. **(B)** Quantitative analysis of cell viability based on image analysis of the live/dead assay. **(C)** Immunofluorescence of hFDM against FN in PVA/hFDM treated with either PBS or 0.1 N HCl. **(D)** Culture of fibroblasts on PBS-treated and 0.1 N HCl-treated PVA/hFDM, respectively. F-actin is stained red and focal adhesion molecule vinculin is shown in green. **(E)** Quantitative analysis of cell spreading area and **(F)** cell density based on image analysis of (D). All scale bars are 50 µm. Cipro: ciprofloxacin; FN: fibronectin; HCl: hydrochloric acid; hFDM: human lung fibroblast-derived matrix; PBS: phosphate buffered saline; PVA: polyvinyl alcohol; TCP: tissue culture plastic.
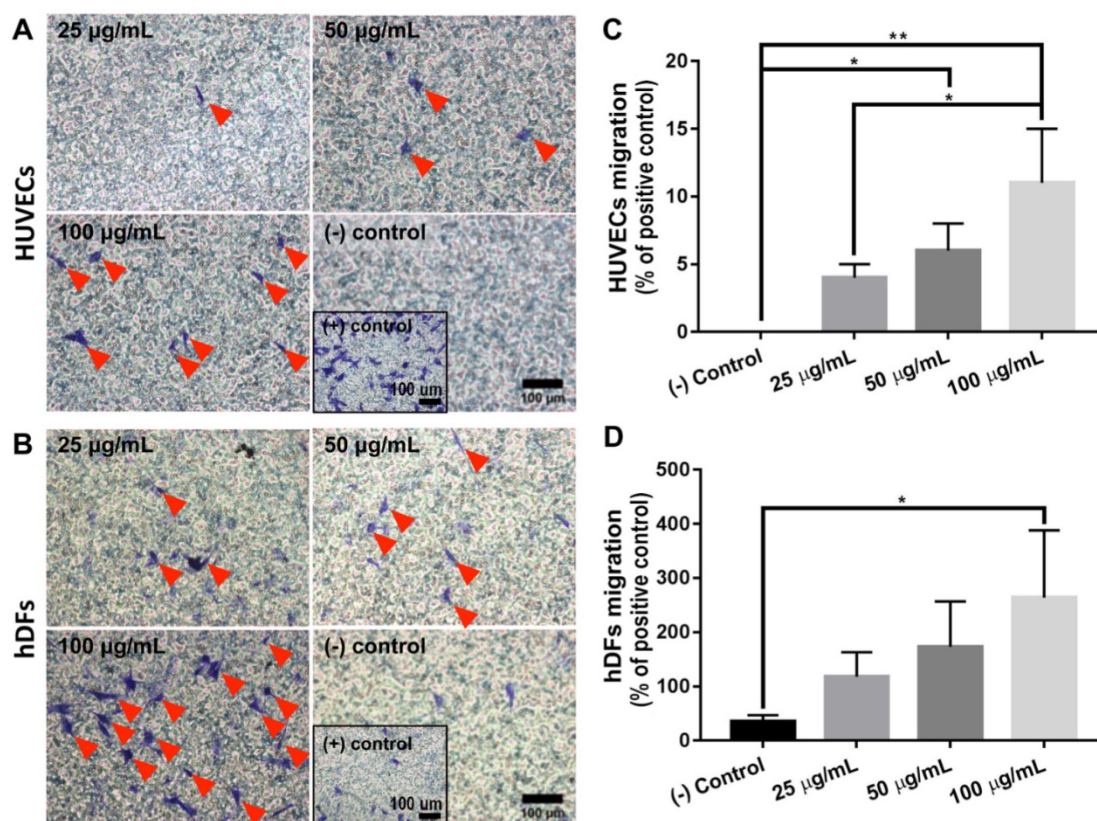
Figure 3. Chemotactic effect of hFDM. (A-B) Migration of HUVECs and HDFs, respectively, treated with different concentrations of hFDM suspension, as evaluated via transwell migration assay. The migrated cells are spotted using crystal violet staining. Red triangles designate migrated cells. Positive and negative controls are 10% FBS and serum-free conditions, respectively. Scale bars are 100 μm. **(C-D)** Quantitative comparison of the number of HUVECs and HDFs migrated through the transwell membrane. The cell number is normalized to that of positive control. Statistically significant difference: *$p < 0.05$ or **$p < 0.01$. HDFs: human dermal fibroblasts; hFDM: human lung fibroblast-derived matrix; HUVECs: human umbilical vein endothelial cells.

Quantitatively analyzed, the chemotaxis effect of hFDM was concentration-dependent, showing more migrated cells with higher contents of hFDM (**Figure 3C-D**). Interestingly, hFDM was much more effective in promoting cell migration with HDFs than HUVECs. The percentage of migrated cells was significantly improved with hFDM suspension compared to even that of the positive control.

Gap junctional communication of HUVECs

Observation of cell-cell communication via intercellular gap junction was carried out via a dye transfer assay that detects cell-to-cell interactions between calcein AM-labeled HUVECs (green) and RFP-HUVECs (red). Calcein dye can only be transferred from one cell to another when those cells directly contact through gap junction connection [17]. In that sense, RFP-HUVECs with calcein dye (green) are considered to be positive in terms of gap junction-mediated intercellular communication (**Figure 4A**). Quantitative analysis of dye transfer into RFP-HUVECs showed a much higher percentage of calcein-positive cells when cells were cultured on hFDM than on gelatin (**Figure 4C**). In order to elucidate this finding further, we examined Cx43, a gap junction protein [18] in the HUVECs; cells on both

substrates showed expression of Cx43 (**Figure 4B**). However the expression level was more upregulated for those on hFDM as confirmed via image analysis, and the difference was statistically significant (**Figure 4D**).

Antibacterial assay *in vitro*

To investigate the antibacterial activity of PVA/Cipro/hFDM via zone inhibition assay, both PVA/Cipro and PVA/Cipro/hFDM were compared against PVA alone (control). The results demonstrated that experimental groups containing ciprofloxacin showed excellent antibacterial activity, as indicated by the zone of inhibition (**Figure S4A-D**). Quantitatively, PVA exhibited a slight inhibition since *E. coli* was previously known to be susceptible to acidic pH [19]. This inhibition zone was much smaller than that of PVA/Cipro or PVA/Cipro/hFDM (**Figure S4E**). For the other strains, the capability of ciprofloxacin-containing PVA membranes to kill bacteria was excellent and comparable, whereas membranes without ciprofloxacin showed no bacterial inhibition (**Figure S4F-H**). These data support the fact that the presence of hFDM in PVA hydrogel has no negative impact on the antimicrobial activity of ciprofloxacin.
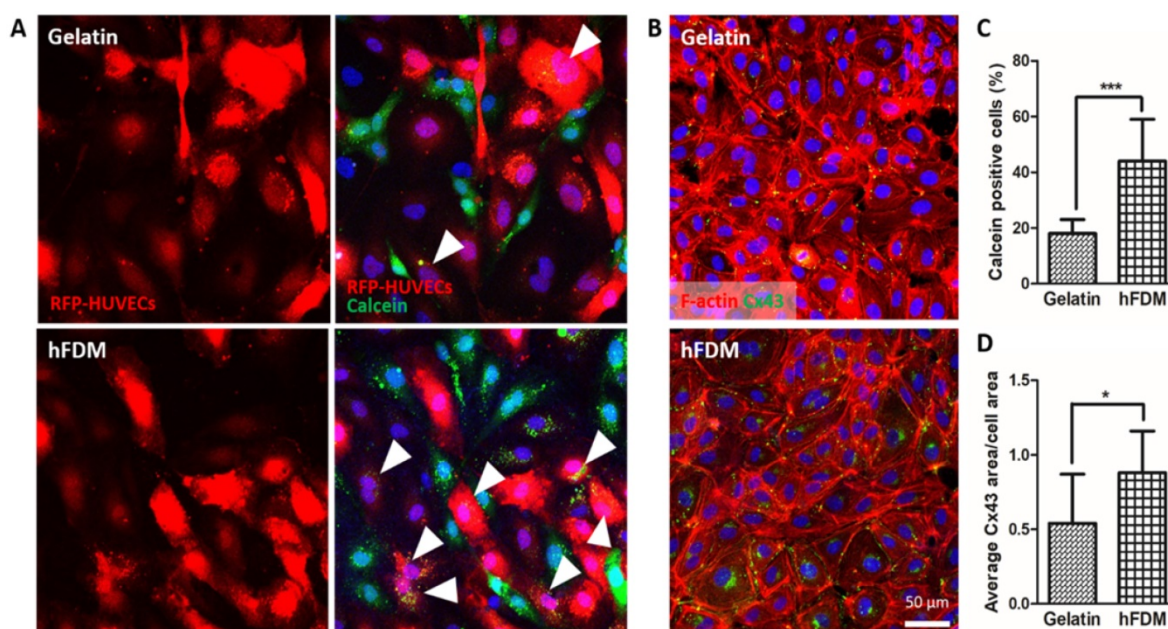
Figure 4. Gap junction-mediated cell-cell communication. (A) Dye transfer assay between calcein AM-labeled HUVECs (green) and RFP-HUVECs (red) after 24 h co-culture on gelatin and hFDM, respectively; the images in the left side show only the RFP-HUVECs, and the merged images of RFP-HUVECs and calcein AM-labeled HUVECs are on the right side. Positive signals (white triangles) are identified via the RFP-HUVECs (red) with green dye (calcein AM) uptake. **(B)** Expression of Cx43 protein (green) with HUVECs cultured on either gelatin or hFDM for 3 days, along with F-actin staining (red). **(C)** Percentage of calcein dye-positive RFP-HUVECs as calculated via image analysis after the dye transfer assay; the percentage was averaged by counting the number of dye-positive RFP-HUVECs against total RFP-HUVECs in a given image. **(D)** Quantitative evaluation of average Cx43 area per cell area. All scale bars are 50 µm. Statistically significant difference: *$p < 0.05$ or ***$p < 0.001$. Cx43: connexin 43; HUVECs: human umbilical vein endothelial cells; RFP-HUVECs: red fluorescence protein expressing HUVECs.

Wound healing: epidermis and dermis regeneration

A skin wound model infected with *S. aureus*, a common bacteria found in infected and non-infected wounds [20], was prepared and subsequently treated with PVA, PVA/Cipro, and PVA/Cipro/hFDM. Infected wound alone served as a control. Of particular interest is the effect of PVA/Cipro/hFDM that holds dual functions from ciprofloxacin, an antimicrobial agent, and hFDM, a supportive microenvironment for wound healing. We assume that the combination of drug and ECM could greatly help facilitate wound healing.

Photographic observation at different time points showed the progression of wound healing with time (**Figure 5A**). Examination on day 3 revealed deposition of pus in the wounds treated without ciprofloxacin (control and PVA). The thick exudates of yellowish opaque liquid are a typical indicator of bacterial infection [21]. Treatments with PVA/Cipro and PVA/Cipro/hFDM exhibited no microbial activity. Bacterial counts taken from wound swabs indicate disappearance of bacterial colonies in the wounds when treated with ciprofloxacin. This is sharply contrasted with control and PVA groups where the number of bacteria is significantly high (**Figure 5B**). The size of the wounds in control, PVA/Cipro, and PVA/Cipro/hFDM groups became

smaller with time (**Figure 5C**). These results demonstrate that wound treatments with ciprofloxacin could heal faster than those without antibiotic. The wound treated with PVA showed poor healing.

For more detailed information about the wound healing progress, excised skin tissues in the wound areas were examined using H&E staining. Wound healing was still incomplete as observed at 15 days by the partial regeneration of the epidermis and dermis layers in all the groups (**Figure S5A**). A closer examination at high magnification shows the regions where the new epidermis appeared (**Figure S5B**); both control and PVA have poorly organized epidermis layers compared to PVA/Cipro and PVA/Cipro/hFDM. Compared to the normal skin, the epidermis layer was relatively very thick in all groups (**Figure S5C**). At 3 weeks post-treatment, reepithelialization and advanced wound healing was apparent. From a macroscopic view, PVA/Cipro/hFDM showed the most promising wound regeneration similar to the unique features of normal skin (**Figure 6A**).

From a microscopic examination, the neoepidermis developed significantly different patterns of regeneration among the tested groups; interestingly neo-dermis from wounds treated with PVA/Cipro/hFDM exhibited signs of skin adnexa (glands, hair follicles), a critical evidence of skin regeneration (**Figure 6B**). It is also notable that the thicknesses of

the epidermis of normal skin and the neoepidermis of the PVA/Cipro/hFDM-treated group were comparable (**Figure 6C**). These findings strongly indicate a significant role of exogenously supplied hFDM in wound healing. Moreover, our results present that control and PVA-treated wounds have a much lower density of microvessels (yellow arrows) than those treated with PVA/Cipro and PVA/Cipro/hFDM (**Figure 6D**). Quantitatively, the microvessels density in the Cipro-loaded groups is similar to the level of normal skin, although in normal skin the microvessels are relatively bigger and more robust (**Figure 6E**). In addition, immunofluorescence of CD31 also suggests the same trend, demonstrating more advanced neovascularization after treatment with PVA/Cipro/hFDM (**Figure S6**).

Wound healing: collagen texture and gap junction protein

In the process of wound recovery, synthesis of collagen and its remodeling take place during cell proliferation and tissue remodeling [6]. Our findings show the development of collagen synthesis and sequential remodeling at different time points. On day 15, collagen is being produced, as identified by blue color from Masson's trichrome staining of whole sections of skin tissue samples (**Figure S7A**). Higher magnification (**Figure S7B**) reveals a large number of

nuclei (black dots) in the dermis region, and this indicates the proliferation phase of fibroblasts and consequently collagen production via fibroblasts [6].

On day 21, the macroscopic images strongly hint at much better skin regeneration with PVA/Cipro/hFDM. It was obvious that collagen deposition is visibly more accumulated in the dermis region for the test groups, except PVA/Cipro/hFDM that shows rather an anisotropic collagen distribution (**Figure 7A**). To our particular interest, the wounds treated with PVA/Cipro/hFDM present a distinct pattern of collagen texture and distribution similar to that of normal skin. Images at higher magnification showed that the collagen organizations of control, PVA, and PVA/Cipro are similar to each other but far from that of normal skin (**Figure 7B**). In a sharp contrast, PVA/Cipro/hFDM developed an organized collagen pattern that is fairly close to that of normal skin.

Injuries always trigger inflammatory reactions and macrophages are deeply involved in the wound healing process. When we examined the macrophages (M0) population and their distribution at week 3, the PVA/Cipro/hFDM-treated group showed much fewer macrophages compared to PVA but a similar level to PVA/Cipro (**Figure S8**). The exact role of hFDM on the macrophage-mediated responses *in vivo* warrants further works.
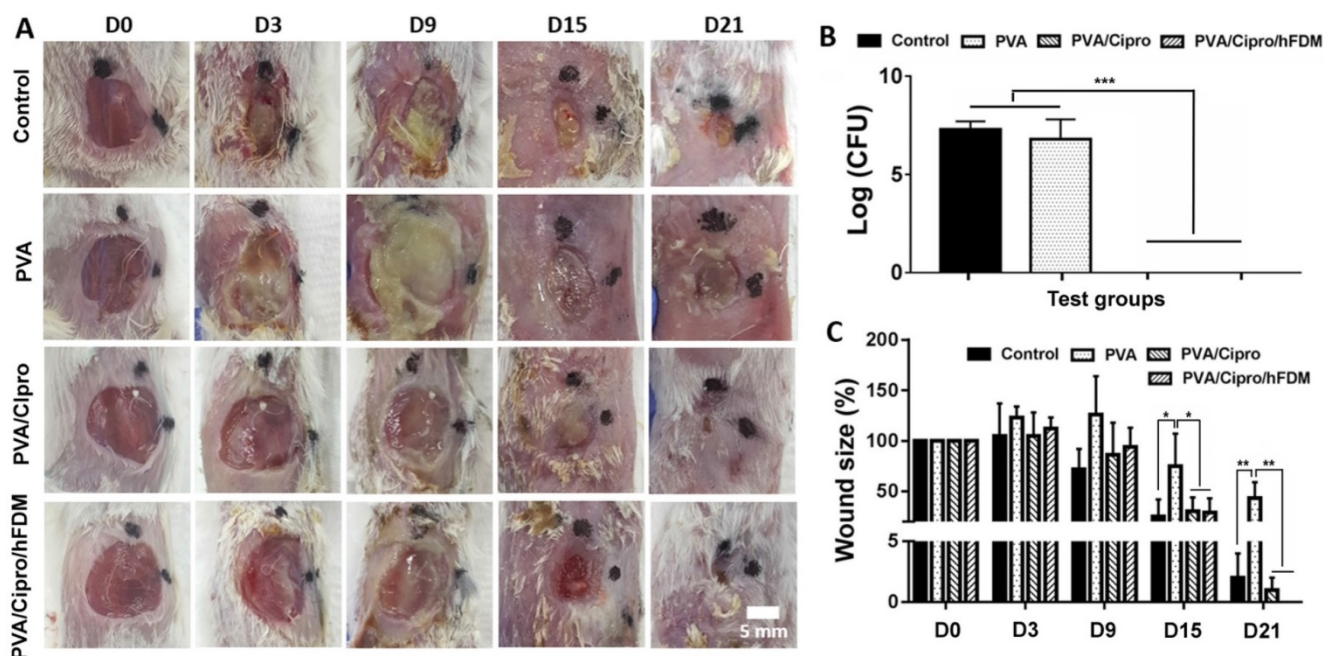

Figure 5. Infected skin wound model and transplantation of PVA-based membranes. (A) Infected wounds on the dorsal region of BABL/c mice and gross appearance of wound closure for up to 21 days (D0-D21). Scale bar is 5 mm. **(B)** Bacterial count (CFU) of the samples collected from the wound sites 6 h post-treatment. **(C)** Measurement of wound size as shown as percentage normalized to that of the initial wound size at day 0. Statistically significant difference: $*p < 0.05$, $**p < 0.01$, or $***p < 0.001$. CFU: colony forming unit; PVA: polyvinyl alcohol.
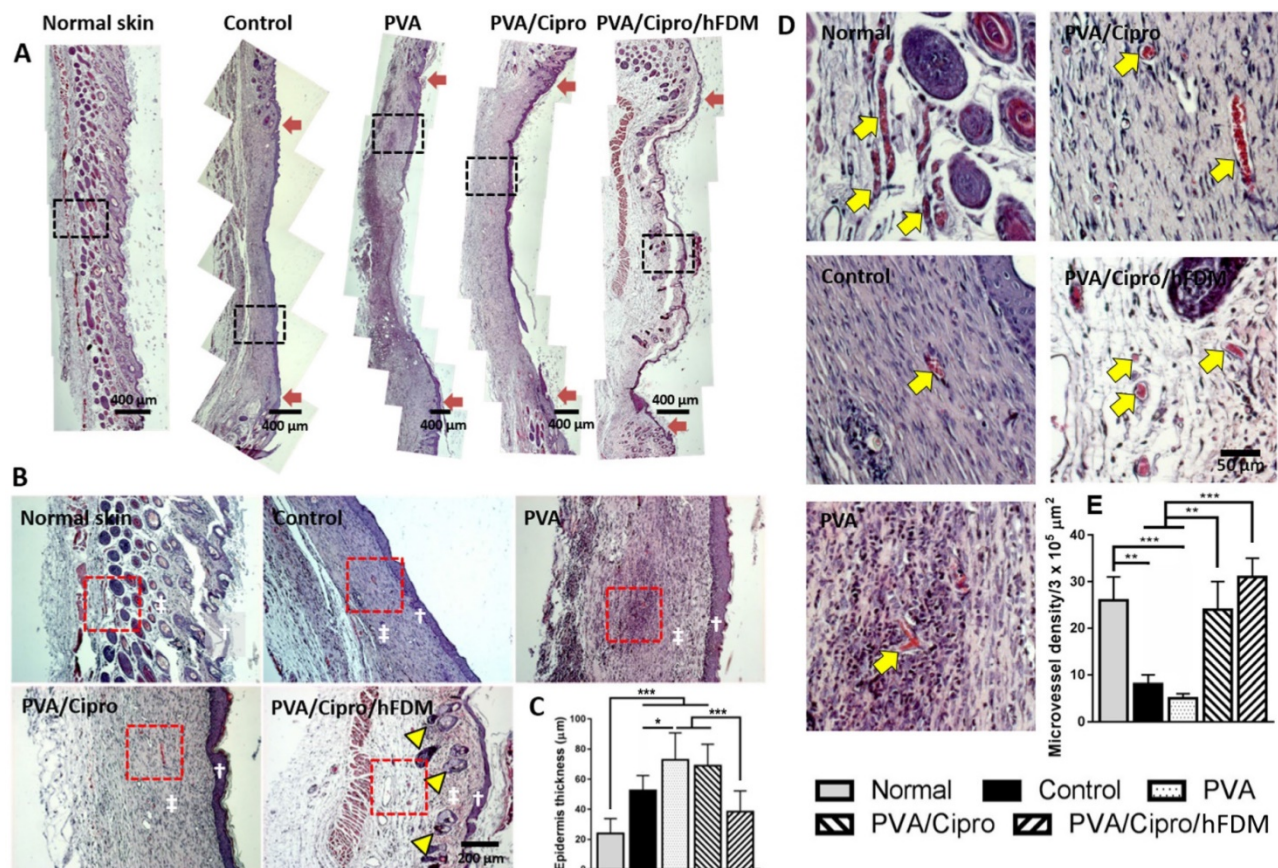
Figure 6. Skin regeneration in epidermis and dermis on day 21. (A) H&E staining of the excised skin tissues collected at 21 days post-treatments. Red arrows indicate the position of the initial wound areas. Dashed black boxes correspond to the enlarged areas shown in (B). Scale bar is 400 μm. **(B)** Higher magnification images of regenerated skin tissues, where white dagger (†) and double dagger (‡) denote the epidermis and dermis layers, respectively. Yellow triangles indicate the regenerated hair follicles and glands. Red boxes indicate the area magnified in (D). Scale bar is 200 μm. **(C)** Thickness of new epidermis. **(D)** Enlarged images show the presence of microvessels in the regenerated dermis as indicated by yellow arrows and the quantitative analysis of microvessel density. Scale bar is 50 μm. Statistically significant difference: *p < 0.05, **p < 0.01 or ***p < 0.001. H&E: hematoxylin and eosin.

Another investigation includes the expression of Cx43, a cell-cell junction protein. Inspection of the whole length of the wounds reveals that the dermis regions of control, PVA, and PVA/Cipro lack Cx43-positive signals. PVA/Cipro/hFDM-treated wound, however, presents considerable amount of Cx43 (**Figure 8A**). Enlarged images of the dermis areas show clear cell organization and Cx43 expression pattern (**Figure 8B**). In normal skin tissue, the unique architecture of skin adnexa, such as glands and follicles, is present along with abundant expression of Cx43 protein. Additionally, the quantitative level of Cx43 expression was found to be much higher in PVA/Cipro/hFDM, as compared to control, PVA, and PVA/Cipro groups (**Figure 8C**). Although tested in *in vitro* conditions, the results in **Figure 4D** support indirectly the positive role of hFDM in improving Cx43 expression.

Discussion

The skin patch reported here was designed with the intention of harnessing the regenerative capability of cell-derived ECM (i.e., hFDM). Our group has been

investigating hFDM as a valuable material source in tissue engineering and regenerative medicine and eventually we intend to transform it into advanced medical devices for wound dressing. hFDM does retain many beneficial assets that could facilitate tissue regeneration as documented in our previous works [22,23]. We have also reported the thickness of fibroblast-derived matrix 1700 ± 250 nm via atomic force microscopy and found major ECM components (fibronectin and collagen type I) in the hFDM [23,24]. Among many different cell types, we selected human lung fibroblasts due to their greater capacity of ECM synthesis *in vitro* over other cells (data not shown).

In this work, a novel skin patch was created via a physically induced coupling of hFDM and bioinert PVA hydrogel, wherein there exists stable and tight contacts at the interface of the two materials. Obviously one of the biggest technical hurdles has been to make the extremely soft cell-derived ECM transferrable while keeping its original architecture and physical form intact. After numerous trials, we were able to establish our own enabling technology to successfully fabricate PVA/hFDM. In fact, various

technologies for wound healing have been explored by incorporating many different aspects, such as natural, modified, or synthetic polymeric materials, as well as nanotechnology or drug delivery systems [25,26]. Incorporation of antibacterial agents into skin patches is also an emerging concept for wound management [27]. To the best of our knowledge, combining a naturally derived ECM and antibiotic molecule in a single hydrogel system as shown in this study has never been reported.

The ability of PVA to hold hFDM on its surface may be attributed to the adhesive nature of PVA hydrogel [28]. Interestingly, formation of this "green-bond" is one of the essential properties of adhesive hydrogels as dressing materials [29]. Another possibility is the physical interactions that enable the formation of a mechanical interlock between hFDM and PVA. In fact, we employed ultrasonication, a very powerful agitation instrument, to evaluate the stability of hFDM. The results show that most of hFDM is intact after repeated ultrasonication treatment (**Figure S3**). Another issue in the fabrication of PVA/hFDM is that there is a concern about FBS contamination during the transfer of hFDM onto PVA; FBS may cause undesirable immunological responses once transplanted. Once decellularized, we rinse the hFDM several times with PBS to get rid of cellular debris and FBS components. In addition, to examine protein adsorption onto hFDM, we incubated hFDM in albumin solution (2 mg/mL) for 12 h and measured the protein contents via BCA assay. The result suggested that the proteins from FBS are rarely adsorbed onto hFDM (data not shown).

The most interesting finding is that advanced wound repair including skin adnexa regeneration (glands, hair follicles) is possible using PVA/Cipro/hFDM, where we observed the critical role of hFDM during wound healing.
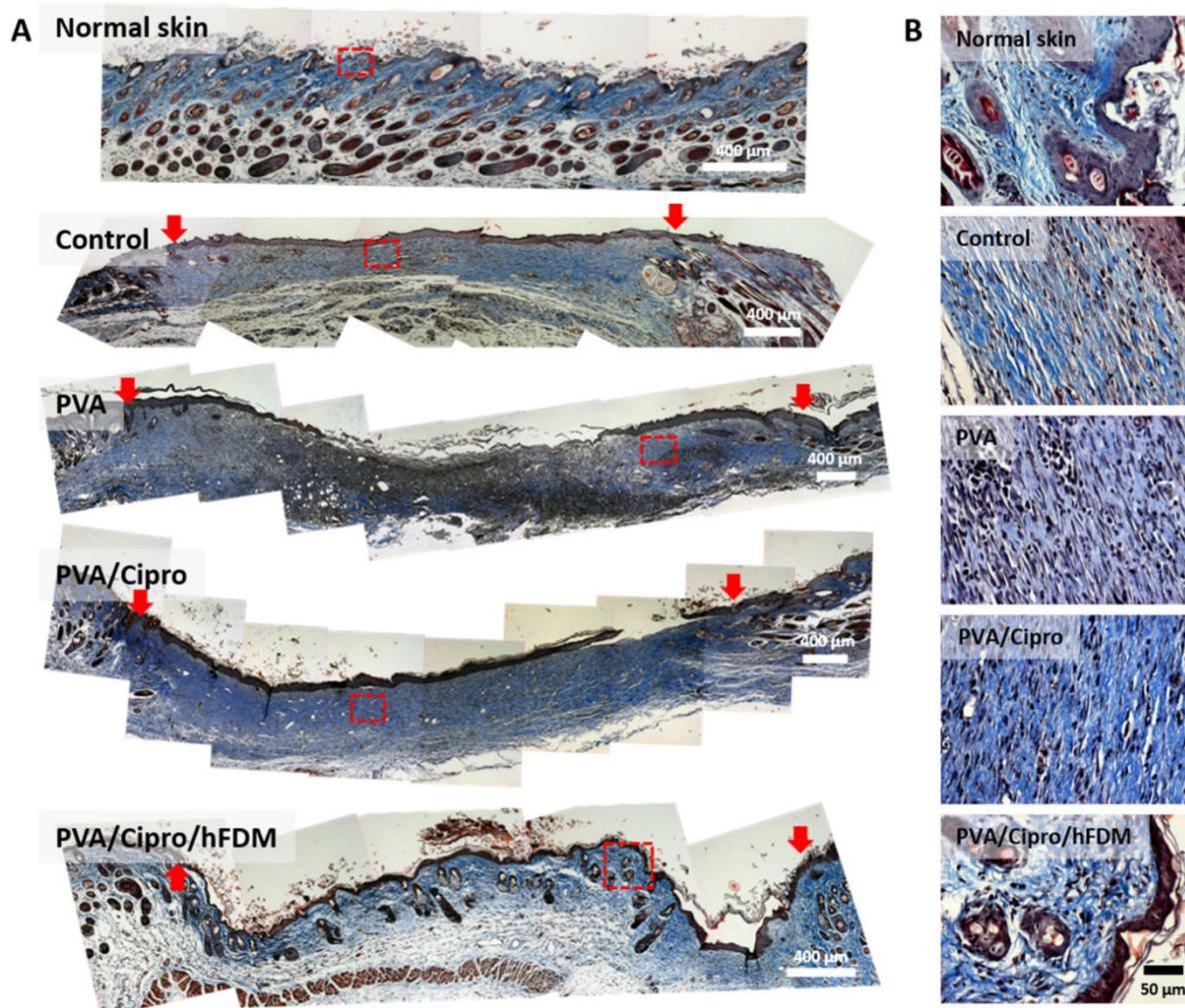

Figure 7. Analysis of collagen texture and distribution pattern on day 21. (A) Masson's trichrome staining of the excised skin tissues on day 21 post-treatments. Collagen and nuclei are indicated by blue color and black dots, respectively. Red arrows indicate the position of the initial wound areas. Dashed red boxes indicate the enlarged areas. Scale bar is 400 μm. **(B)** Higher magnification images show deposition of collagen and their distribution pattern in the epidermis and dermis. Scale bar is 50 μm.
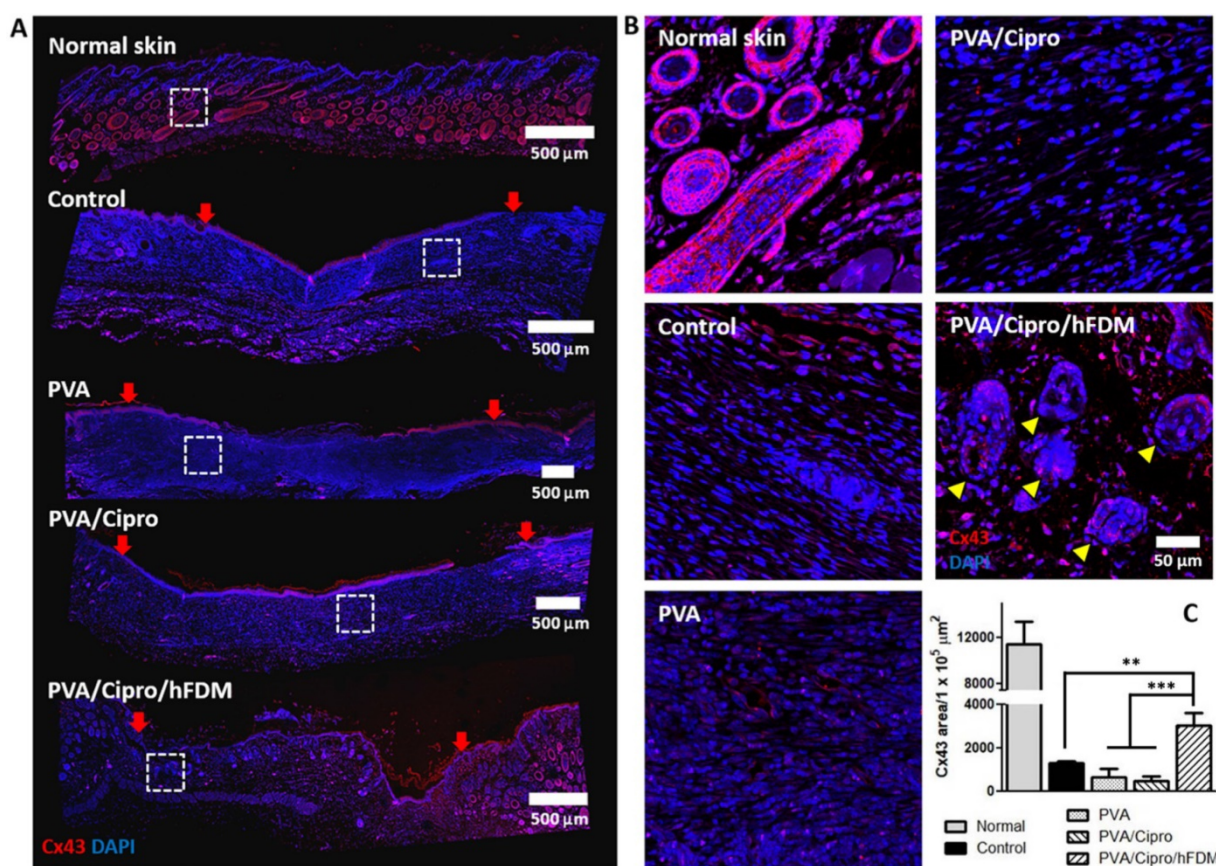
Figure 8. Analysis of gap junction protein expression. (A) Immunofluorescence of Cx43 protein with the skin tissues retrieved at 21 days post-treatments. Cx43 and nuclei (DAPI) are indicated in red and blue color, respectively. Red arrows show the position of the initial wound regions. Dashed white boxes indicate the magnified areas. Scale bar is 500 μm. **(B)** Higher magnification images present the expression and organization of Cx43 protein in the regenerated dermis. Yellow triangles indicate the regenerated follicles and glands. Scale bar is 50 μm. **(C)** Quantitative analysis of Cx43-positive area per unit area (1×10^5 μm²). Statistically significant difference among control, PVA, PVA/Cipro and PVA/Cipro/hFDM: $**p < 0.01$ or $***p < 0.001$. Cipro: ciprofloxacin; Cx43: connexin 43; DAPI: 4', 6-diamidino-2-phenylindole; hFDM: human lung fibroblast-derived matrix; PVA: polyvinyl alcohol.

Previous reports showed that ECM molecules, such as collagen, fibronectin, proteoglycan, and laminin, are critical components for cutaneous wound healing [30,31], let alone growth factors and cells. Although the exact role of hFDM in wound healing is unclear at this time, there are a few presumable scenarios, including the intrinsic potential of hFDM on angiogenesis. Our previous experiences strongly suggest the highly beneficial impact of hFDM on capillary-like structure formation on 2D substrate as well as in 3D environments [23,24]. We found that hFDM itself contains many angiogenic factors, such as basic fibroblast growth factor and hepatocyte growth factors among others [23]. Our study also noticed that new blood vessel formation was more active in the regenerated tissue when treated with PVA/Cipro/hFDM. Angiogenesis is an essential process that provides the regenerating tissue with nutrients and oxygen during the tissue repair process [32]. Regarding the new blood vessels, higher expression of gap junction protein in the presence of hFDM may explain the better neovascularization as shown in **Figure 4D** and **Figure 8C**. Among the gap

junction proteins, Cx43 is the most common one in the skin tissue and plays a major role in the process of wound healing, such as dermal fibroblast migration [33]. Cx43 is also crucial in the wound healing stage because this protein is needed for vascularization of endothelial cells and angiogenesis [34,35]. Additionally our early studies support much upregulated expression of Cx43 on hFDM with a different cell type, cardiomyoblasts (H9c2), over fibronectin, a typical ECM molecule [14,33].

Moreover, the advanced wound regeneration via PVA/Cipro/hFDM can be explained by enhanced gap junction intercellular interactions at the wound site. The role of gap junction protein Cx43 in the wound healing process has been well documented [36]. One example is smooth transfer of oxygen and nutrients to the cells. The establishment of intercellular gap junction-mediated communications is deeply involved in the maturation of granulation tissue. This type of cell-cell crosstalk also directs the orientation of collagen-producing fibroblasts that in the end affect the arrangement of collagen fiber bundles [37] and restoration of dermal

histoarchitecture [38]. Obviously, well-organized development of ECM architecture is a crucial aspect during the wound healing process.

On the other hand, investigations about the chemotactic effect of hFDM *in vitro* showed an interesting finding in a sense that its chemotactic properties are dependent on concentration as well as being cell type specific. Even though the exact reason why hFDM serves as a chemoattractant warrants further investigation, it is well known that multiple growth factors are responsible for inducing cell migration, such as platelet-derived growth factor-AB and insulin-like growth factor 1 [39]. ECM-growth factors interactions also have crucial roles, including growth factors binding, release, and protection [40]. Upon enzymatic digestion of hFDM by pepsin, however, it is reasonable to postulate that the bioactivity of such growth factors would be significantly compromised. In that sense, the digested hFDM fragments might play a role in guiding chemoattractant effects, such as those in the hydrolyzed porcine small intestinal submucosa (SIS). Li et al. suggested that small molecular weight peptides derived from the degraded porcine SIS are biologically active in the recruitment of murine endothelial cells [41]. In fact, ECM fragments generated by proteolytic enzymes are called matrikines and they are considered active components that interact with cell surface receptors for downstream cell signaling.

For infected wound treatment, ciprofloxacin-loaded PVA was prepared and evaluated for its release profile *in vitro*. In a polymer system such as PVA hydrogel, the release kinetic of entrapped drug is mainly diffusion-based [42]. In correlation to initial loading contents, more drug molecules inside the polymer creates a higher concentration gradient between the inside and outside systems, leading to a faster drug diffusion rate [43]. This may explain the linear correlation between initial ciprofloxacin loading concentration and release rate *in vitro*. It is notable, however, that regardless of the loading concentrations, most of the drug was released within 2 h and this release pattern can be faster in *in vivo* conditions. While it may be dependent of the severity of the contaminated wounds, we consider 2 h a sufficient time to kill the bacteria when the skin patch is replaced twice a week. Based on the 8% loading efficiency, we identified 10 mg/mL ciprofloxacin as an optimal, conservative dose that would have sufficient effect and minimal adverse reaction *in vivo*.

The ciprofloxacin-loaded patch showed excellent antibacterial effect against four bacterial strains (gram-negative and -positive). Ciprofloxacin (a synthetic second-generation quinolone antibiotic) has been shown to be efficacious against gram-negative and -positive aerobic bacteria as well as several strains of anaerobic gram-negative species. This drug targets topoisomerases that affect DNA replication, cell division, and ATP generation, among others [44]. Our results suggest that ciprofloxacin has a wide range of antibacterial activity against gram-negative and -positive bacteria and that ciprofloxacin-loaded PVA/hFDM (PVA/Cipro/hFDM) proves its feasibility with excellent antibacterial activity. As demonstrated from our animal study, the antibacterial property of this drug can also be very effective *in vivo* when combined with our skin patch. It is mentionable that the wound treated with PVA had a lower capability of wound closure, even when compared to the untreated group (control). We postulate that PVA itself provides a humid environment for bacterial growth so that it slows down the wound healing process. However, the presence of ciprofloxacin could overcome this phenomenon.

Conclusions

In this study, a novel skin patch combining both antibiotic ciprofloxacin and cell-derived ECM was fabricated via coupling with biocompatible, elastic PVA hydrogel. We found that hFDM was securely anchored to PVA and ciprofloxacin was successfully incorporated into the system. In vitro analysis demonstrates the benefits of hFDM in supporting cell migration and in establishing gap junctional communication. Ciprofloxacin proved to be very effective against gram-negative and -positive bacteria. An animal study using an infected wound model supports the importance of antibacterial activity for wound healing. Among the test groups, PVA/Cipro/hFDM showed the most advanced wound regeneration as identified by a thin layer of re-epithelialization, distinct collagen texture and distribution, neovascularization, along with regenerated glands and hair follicles in the dermis. Taken together, the combination of antibiotic and ECM in the form of PVA/Cipro/hFDM can be an effective strategy in putting two essential factors together into a single membrane. This system should be a promising candidate in treating infected wounds for advanced skin regeneration and can find diverse applications in the area of tissue engineering.

Abbreviations

BSA: bovine serum albumin; CFU: colony forming unit; Cipro: ciprofloxacin; Cx43: connexin 43; DAPI: 4', 6-diamidino-2-phenylindole; DMEM: Dulbecco's modified Eagle's medium; ECM: extracellular matrix; FBS: fetal bovine serum; FN:

fibronectin; HCl: hydrochloric acid; HDFs: human dermal fibroblasts; H&E: hematoxylin and eosin; hFDM: human lung fibroblast-derived matrix; HUVECs: human umbilical vein endothelial cells; PBS: phosphate buffered saline; PVA: polyvinyl alcohol; RFP-HUVECs: red fluorescence protein expressing HUVECs; SIS: small intestinal submucosa; TCP: tissue culture plate.

Supplementary Material

Supplementary figures.
http://www.thno.org/v08p5025s1.pdf

Competing Interests

The authors have declared that no competing interest exists.

References

1. Deng CM, He LZ, Zhao M, et al. Biological properties of the chitosan-gelatin sponge wound dressing. Carbohydr Polym. 2007; 69: 583–89.
2. Guo S, Dipietro LA. Factors affecting wound healing. J Dent Res. 2010; 89: 219–29.
3. Fan Z, Liu B, Wang J, et al. A novel wound dressing based on Ag/graphene polymer hydrogel: effectively kill bacteria and accelerate wound healing. Adv Funct Mater. 2014; 24: 3933–43.
4. Zilberman M, Egozi D, Shemesh M, et al. Hybrid wound dressings with controlled release of antibiotics: structure-release profile effects and in vivo study in a guinea pig burn model. Acta Biomater 2015; 22: 155–63.
5. Chester D, Brown AC. The role of biophysical properties of provisional matrix proteins in wound repair. Matrix Biol. 2017; 60–61: 124–40.
6. Schultz GS, Wysocki A. Interactions between extracellular matrix and growth factors in wound healing. Wound Repair Regen. 2009; 17: 153–62.
7. Kim EJ, Choi JS, Kim JS, et al. Injectable and thermosensitive soluble extracellular matrix and methylcellulose hydrogels for stem cell delivery in skin wounds. Biomacromolecules. 2016; 17: 4–11.
8. Choi JS, Kim JD, Yoon HS, et al. Full-thickness skin wound healing using human placenta-derived extracellular matrix containing bioactive molecules. Tissue Eng Part A. 2013; 19: 329–39.
9. Guan Y, Qi XM, Chen GG, et al. Facile approach to prepare drug-loading film from hemicelluloses and chitosan. Carbohydr Polym. 2016; 153: 542–48.
10. Fitzpatrick LE, McDevitt TC. Cell-derived matrices for tissue engineering and regenerative medicine applications. Biomater Sci. 2015; 3: 12–24.
11. Zhou G, Ruhan A, Ge H, et al. Research on a novel poly (vinyl alcohol)/lysine/vanillin wound dressing: biocompatibility, bioactivity and antimicrobial activity. Burns. 2014; 40: 1668–78.
12. CLSI. Performance standards for antimicrobial disk susceptibility tests. CLSI standard M02, 9th ed. Wayne, Pennsylvania: Clinical and Laboratory Standards Institute; 2006.
13. Kopecki Z, Ogunniyi AD, Trott DJ, et al. Fighting chronic wound infection – one model at a time. Wound Practice and Research. 2017; 25: 6–13.
14. Suhaeri M, Subbiah R, Van SY, et al. Cardiomyoblast (H9c2) differentiation on tunable extracellular matrix microenvironment. Tissue Eng Part A. 2015; 21: 1940–51.
15. Hou Y, Chen C, Liu K, et al. Preparation of PVA hydrogel with high-transparence and investigations of its transparent mechanism. RSC Adv. 2015; 5: 24023–30.
16. Choi DH, Suhaeri M, Hwang MP, et al. Multi-lineage differentiation of human mesenchymal stromal cells on the biophysical microenvironment of cell-derived matrix. Cell Tissue Res. 2014; 357: 781–92.
17. Ryu S, Yoo J, Jang Y, et al. Nanothin coculture membranes with tunable pore architecture and thermoresponsive functionality for transfer-printable stem cell-derived cardiac sheets. ACS Nano. 2015; 9: 10186–202.
18. Guillotin B, Bourget C, Remy-Zolgadri M, et al. Human primary endothelial cells stimulate human osteoprogenitor cell differentiation. Cell Physiol Biochem. 2004; 14: 325–32.
19. Zhu H, Hart CA, Sales D, et al. Bacterial killing in gastric juice - effect of pH and pepsin on escherichia coli and helicobacter pylori. J Med Microbiol. 2006; 55: 1265–70.
20. Hampton S. Bacteria and wound healing. J Community Nurs. 2007; 21: 32–40.
21. Healy B, Freedman A. Infections. BMJ. 2006; 332: 838–41.
22. Kim IG, Hwang MP, Du P, et al. Bioactive cell-derived matrices combined with polymer mesh scaffold for osteogenesis and bone healing. Biomaterials. 2015; 50: 75-86.
23. Du P, Suhaeri M, Ha SS, et al. Human lung fibroblast-derived matrix facilitates vascular morphogenesis in 3D environment and enhances skin wound healing. Acta Biomater. 2017; 54: 333-44.
24. Du P, Subbiah R, Park JH, et al. Vascular morphogenesis of human umbilical vein endothelial cells on cell-derived macromolecular matrix microenvironment. Tissue Eng Part A. 2014; 20 (17-18): 2365-77.
25. Moura LIF, Dias AMA, Carvalho E, et al. Recent advances on the development of wound dressings for diabetic foot ulcer treatment—a review. Acta Biomater. 2013; 9: 7093–7114.
26. Mayet N, Choonara YE, Kumar P, et al. A comprehensive review of advanced biopolymeric wound healing systems. J Pharm Sci. 2014; 103: 2211–30.
27. Simões D, Miguel SP, Ribeiro MP, et al. Recent advances on antimicrobial wound dressing: a review. Eur J Pharm Biopharm. 2018; 127: 130–41.
28. Cha W, Hyon S, Graiver D, et al. Sticky poly(vinyl alcohol) hydrogels. J Appl Polym Sci. 1993; 47: 339–43.
29. Ben-Zion O, Karpasas M, Nussinovitch A. Determination of green-bond strength in tacky poly(vinyl alcohol) hydrogels. J Appl Polym Sci. 2003; 87: 2130–35.
30. Macri L, Clark RAF. Tissue engineering for cutaneous wounds: selecting the proper time and space for growth factors, cells and the extracellular matrix. Skin Pharmacol Physiol. 2009; 22: 83–93.
31. Olczyk P, Mencner Ł, Komosinska-Vassev K. The role of the extracellular matrix components in cutaneous wound healing. Biomed Res Int. 2014; 2014: 747584.
32. Eming SA, Martin P, Tomic-Canic M. Wound repair and regeneration: mechanisms, signaling, and translation. Sci Transl Med. 2014; 6: 265sr6.
33. Churko JM, Laird DW. Gap junction remodeling in skin repair following wounding and disease. Physiology. 2013; 28: 190–98.
34. Wang HH, Su CH, Wu YJ, et al. Reduction of connexin43 in human endothelial progenitor cells impairs the angiogenic potential. Angiogenesis. 2013; 16: 553–60.
35. Gärtner C, Ziegelhöffer B, Kostelka M, et al. Knock-down of endothelial connexins impairs angiogenesis. Pharmacol Res. 2012; 65: 347–57.
36. Ehrlich HP, Diez T. Role for gap junctional intercellular communications in wound repair. Wound Repair Regen. 2003; 11: 481–9.
37. Zylberberg L, Bereiter-Hahn J, Sire J-Y. Cytoskeletal organization and collagen orientation in the fish scales. Cell Tissue Res. 1988; 253: 597–607.
38. Ghatnekar GS, O'Quinn MP, Jourdan LJ, et al. Connexin43 carboxyl-terminal peptides reduce scar progenitor and promote regenerative healing following skin wounding. Regen Med. 2009; 4: 205–23.
39. Ponte AL, Marais E, Gallay N, et al. The in vitro migration capacity of human bone marrow mesenchymal stem cells: comparison of chemokine and growth factor chemotactic activities. Stem Cells. 2007; 25: 1737–45.
40. Hynes RO. The Extracellular matrix: not just pretty fibrils. Science. 2009; 326: 1216–19.
41. Li F, Li W, Johnson SA, et al. Low-molecular-weight peptides derived from extracellular matrix as chemoattractants for primary endothelial cells. Endothelium. 2004; 11: 199–206.
42. Gutiérrez MC, García-Carvajal ZY, Jobbágy M, et al. Poly(vinyl alcohol) scaffolds with tailored morphologies for drug delivery and controlled release. Adv Funct Mater. 2007; 17: 3505–13.
43. Abdekhodaie MJ, Wu XY. Drug release from ion-exchange microspheres: mathematical modeling and experimental verification. Biomaterials. 2008; 29: 1654–63.
44. Kohanski MA, Dwyer DJ, Collins JJ. How antibiotics kill bacteria: from targets to networks. Nat Rev Microbiol. 2010; 8: 423–35.